International Journal of Civil Engineering

Structure
Concrete

Load displacement behavior of concrete beam under monotonic static and low velocity impact load

M. C. Yilmaz[1], Ö. Anil[2,*], B. Alyavuz[2], E. Kantar[3]

Received: May 2013, Revised: August 2013, Accepted: January 2014

Abstract

Experiments were carried out to observe the influence of loading type on concrete beam specimens. Beam specimens made of similar concrete mixture with the same geometry were tested under three point static loading and low velocity drop weight impact loading. Load – displacement behavior, absorbed energy dissipation capacity, stiffnesses, failure modes of beam specimens were obtained and discussed. A finite element (FE) model was prepared in ANSYS Explicit STR software and the results of FE analysis were compared with experimental results. The loading type and loading rate have significant influence on the maximum load, stiffness and energy dissipation capacity. Numerical results obtained from ANSYS Explicit STR FE models are consistent with the experimental results.

Keywords: *Load- displacement behavior, Concrete beam, Low velocity impact behavior, Drop weight, ANSYS.*

1. Introduction

Among the various effects such as earthquake, wind, machine vibrations, blast related shocks, avalanche, rock fall and high or low velocity object impacts on concrete structures, the impact loads are relatively less studied and known group of dynamic loading. With the short duration of loading and its quite large instantaneous intensity, the impact creates loads changing the mechanical response parameters of concrete such as strength and ductility [1, 2]. Studies on the impact behavior of this material have become a necessity to improve the design of structures like military defense structures or nuclear plants which has a significant influence on a wide range of people.

Various experimental studies on impact response of steel, reinforced concrete (RC), carbon fiber reinforced polymer (CFRP) strengthened or fiber mixed concrete, and composites structures have been presented in the literature. Notable effort has been mainly made on the study of impact response of RC beams, slabs, walls, frames among which beams are the most studied structural member because of its wide usage area [3-11].

These studies usually investigate the differences between mechanical behavior of the member under static and dynamic loading and present some simple equations to predict certain characteristics. For example, a triangular relation between the reaction force – mid length displacement of RC beams without shear reinforcements and a simple equation for the required static shear capacity of the RC beam against the impact load were presented by Kishi et al. through some drop weight impact experiments [3]. A 3d finite element (FE) LS-Dyna model in addition to the drop weight impact experiments on RC beams with variable shear rebar ratio and impact velocity of drop weight were presented by Bhatti et al. [4]. Reaction force, mid span displacement and crack pattern comparisons between FE analysis and experimental results were presented. The response of RC beams to impact loads by Cotsovos et al. [5] using ANSYS finite element software shows that the material properties, which are independent of strain rate, capable to capture the response of RC beam under impact loading. The increase in loading rate increases the load carrying capacity reducing the effective length and maximum deflection of the beam. The shear force carrying capacity for a RC beam using a simplified method which accounts the shear wave velocity, the travel time between load and upper face crack, effective length of the beam and uniaxial compressive strength of the concrete has been formulated by the same author [6].

The experimental study was carried out using a drop weight test setup which had been used in a former study to observe the impact behavior of concrete beams strengthened with CFRP strips [12]. Similar test setups were also used by other researchers to test the concrete beams in a limited number of work [13-14]. Similarly, in these works, a comparison between response of concrete beams to the static loading and the dynamic loading was

** Corresponding author: oanil@gazi.edu.tr*
1 Ph. D, Candidate, Research Assistant of Civil Engineering Department, Gazi University, Maltepe, Ankara, Türkiye
2 Ph. D, Association Professor of Civil Engineering Department, Gazi University, Maltepe, Ankara, Türkiye
3 Ph. D, Assistant Professor of Civil Engineering Department, Celal Bayar University, Manisa, Türkiye

carried out. For example, the failure modes, flexural toughness, and energy absorption mechanisms of railway prestressed concrete sleepers under static and impact loads were presented by Kaewunruen and Remennikov [13]. A simplified approach to predict ultimate moment capacity of prestressed concrete sleepers under impact loading was also presented. Notched concrete samples were tested by Zhang et al. using a similar experimental setup, and fracture work and loading rate relation were represented [14]. Other forms of plain concrete such as concrete cylinders [15] under low velocity impact, and high velocity impact tests on concrete plates [16, 17] can also be found in the literature.

The presented work here includes a numerical analysis in a widely used FE software ANSYS. A drop weight simulation for plain concrete using FE software ABAQUS has been also presented by Kantar et al. [18] comparing the acceleration-time graphs and stress distributions obtained from the numerical simulations and experiments which were carried out for ten specimens of normal and high strength concrete beams with different drop heights. It was indicated that the simulations should only be used for pre-design of the impact behavior of concrete beam. A contact - impact FE formulation which was solved using the Gauss-Seidel iterative algorithm has been presented by Travaš et al [19]. The behavior of material was characterized by a microplane model which is a modification of the model presented by Bazant and Prat [20, 21]. The details of finite strain formulation of microplane model can be found in Bazant et al. [22] and Ozbolt et al. [23]. Transitions between failure modes such as bending failure mode and shear failure mode with respect to drop weight velocity were presented as a result of finite element simulations. The influence of size of the concrete beam at high strain rates was also indicated.

In the present work, concrete beam specimens with the dimensions of 710x150x150 mm were tested under three point static loading and drop weight impact loading. Absorbed energy capacity, stiffnesses, failure modes of beam specimens were observed and discussed. Numerical solution was carried out using Explicit STR in ANSYS FE software and certain parameters such as displacement, velocity, acceleration and stress distribution were compared with experimental results. In this study, the effects of type and velocity of the loading on behavior of RC beams were investigated and the differences between the static and dynamic impact loading were obtained. The impact hammer was dropped from different heights and variable energies were transferred to specimen for comparing with static loading. In addition finite element analyses results were compared and model was verified and compatibility of both results was investigated. Preparation of models that were used during design was aimed.

2. Experimental Study

Six plain concrete beam specimens with the dimensions of 710x150x150 mm were tested under static and low velocity impact loading. Load type and the height of hammer were chosen as variables during the experiments. One of the specimens was tested under three point static loading and the others were tested using drop weight impact test setup with a 5.25 kg steel hammer. The geometry and the support conditions shown in Fig. 1 are equivalent for all specimens. The properties of specimens such as drop height, travel time of hammer up to the impact instant, compressive strength of concrete and failure drop numbers are given in Table 1.

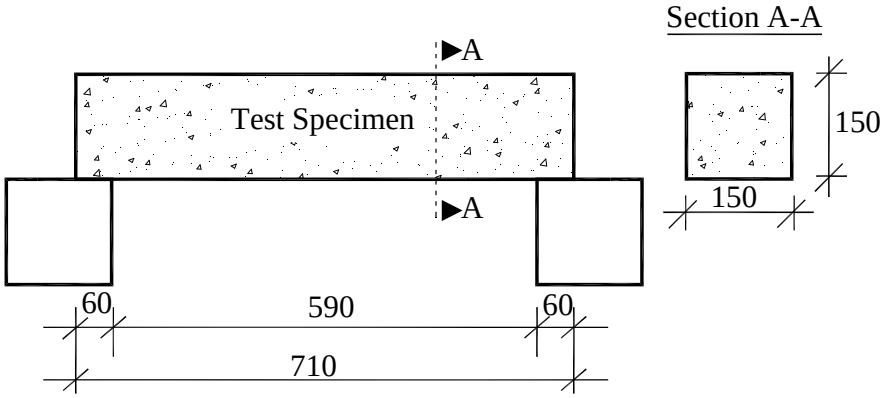

Fig. 1 Dimensions of Test Specimens

Table 1 Test Specimens

Spec. No	Loading Type	Drop Height (mm)	Travel Time (sec)	Failure Drop Number	Concrete Compressive Strength (MPa)
1 (S1)		300	0.235	5	24.86
2 (S2)		350	0.262	4	24.36
3 (S3)	Impact	400	0.286	4	24.72
4 (S4)		450	0.297	2	25.00
5 (S5)		500	0.314	2	24.58
6 (BS1)	Static	-----	-----	-----	24.63

The concrete beams were prepared at the same time using the same concrete mixture. Five cylinder samples of

150x300 mm were also prepared from the same mixture for each specimen to determine the compressive strengths of these beams from axial compression tests. The average values of concrete compressive strengths of the specimens are also presented in Table 1. The correlations between the compressive strengths of concrete specimens are quite high. The static and impact tests were started after the concrete beams had gained their 28 days concrete strength.

2.1 Test setup and instrumentation

The type of loading was used as a parameter in the experiments so that two different test setups were prepared. Static loading tests were carried out using a standard flexure text setup shown in Fig. 2a with three-point loading. Impact tests were carried out using a low velocity drop weight test setup shown in Fig. 2b.

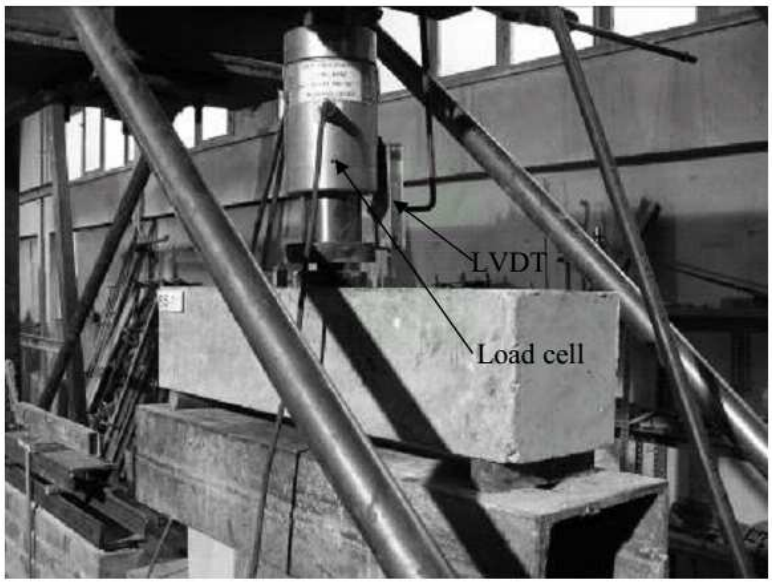

a) Static Test Setup (BS-1 Specimen before Test)

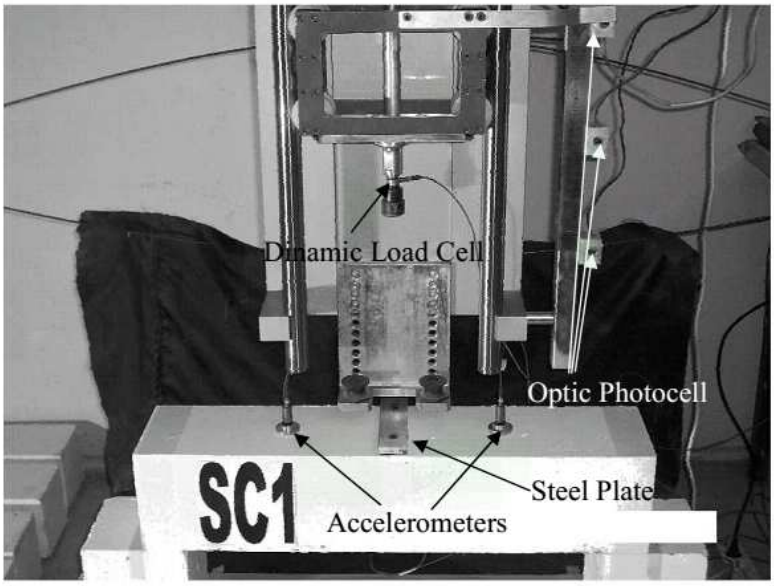

b) Impact Test Setup (S1 Specimen before Test)

Fig. 2 Specimens before Test

The examples of drop weight test setup in the literature have been designed to admit the usage of different drop heights and hammer weights. In the present work, dimensions of the impact test setup and weight of the hammer were determined after inspecting these examples. The eccentricity which has a significant influence on the result of impact tests has been minimized by means of some preliminary drop tests. As a result of these tests, weight of the steel base of test setup was increased to eliminate the eccentricity. The base was manufactured from a square steel plate of 1000 x 1000 mm with a mass of 1000 kg. The details of the designed equipment are shown in Fig. 3. The test setup has the capability of dropping variable weights from 2500 mm. The hammer of

5.25 kg mass was used throughout the experiments. Drop height is changed between 300 mm to 500 mm. The impact test repeated until the failure of concrete specimen at all drop height levels. Another factor influencing the test results is the friction between the guide and the roller, which is reduced by using hard chrome coated grinded rods and cestamide roller during free fall.

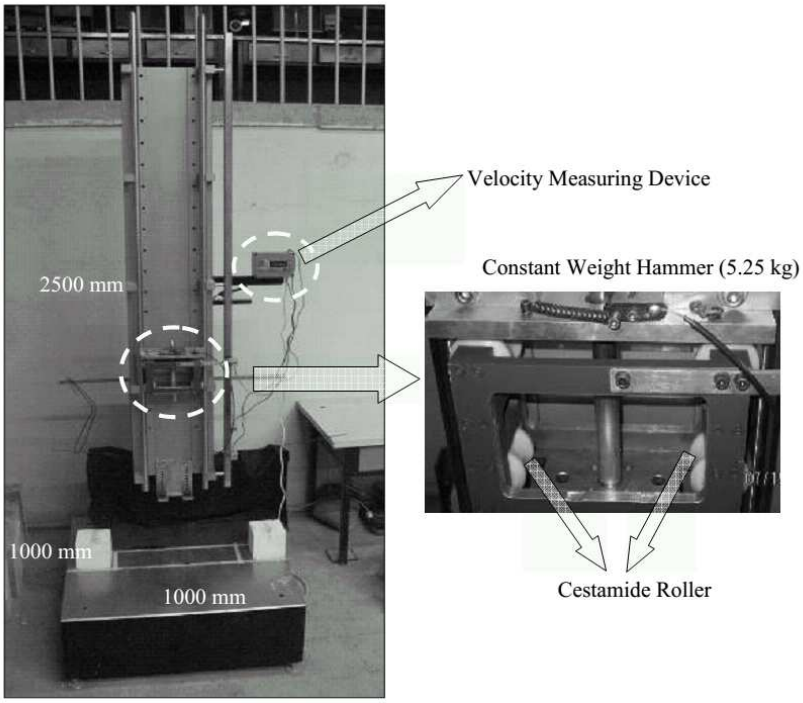

Fig. 3 Impact Test Setup

Initial contact during the impact occurs between the hammer and a steel plate that is supported with a hard rubber cushion. Purpose of using the steel plate is to distribute the load linearly and uniformly to the cross section of the specimen. For minimizing the internal forces, hard rubber is used between the specimen and steel plate. Dimensions of the steel plate and rubber are 50×150×15 in mm. The steel plate with rubber bearing is fixed to the specimen by using steel dowels. A velocity measuring device is placed on the test setup to determine the impact velocity of the hammer. This device uses optical photocells which measure the travel time of hammer from which the velocity can be calculated.

Two accelerometers are mounted on the top surface of each specimen using a brass apparatus and steel dowels shown in Fig. 4. They are located along the longitudinal symmetry axis and 150 mm apart from the symmetry center. ICP type accelerometers have been manufactured by PCB Group with a model number 353B02 (Fig. 5a). The data obtained from these accelerometers are transferred to a computer by means of a data logger. A 003A20 model special cable shown in Fig. 5b, manufactured by PCB Group, was used for the transmission of measurements acquired from the accelerometers to data logger without any data loss. These are low noise, coaxial cables that are suitable for operating at high temperatures and for transmission of high or low impedance voltage signals with ICP sensors. The diameters of the cables are 2 mm and the operation temperature range is between -90 and +260°C. Impedance of the cable is 50 ohm. N1 9233-USB-9162 model data logger manufactured by National Instruments Company was used for collecting the measurements and transmitting to the computer (Fig. 5c). This data logger is a four channel dynamic signal acquisition unit and is composed of IEPE sensors which can acquire measurements with high accuracy. The data logging device is composed of two independent modules. The first module is the data logger to which the measurement devices are also connected. The second is the signal transmission module, which transmits the signal from the first module to computer. Data transferred to computer from data logger is stored after conversion to the required type via Labview Signal Express 3.5 software, developed by National Instrument Company. Calibrations of the measurement devices are performed using this software as well. Diadem 10.1 software, also developed by National Instruments, was used for necessary editing operations during data processing.

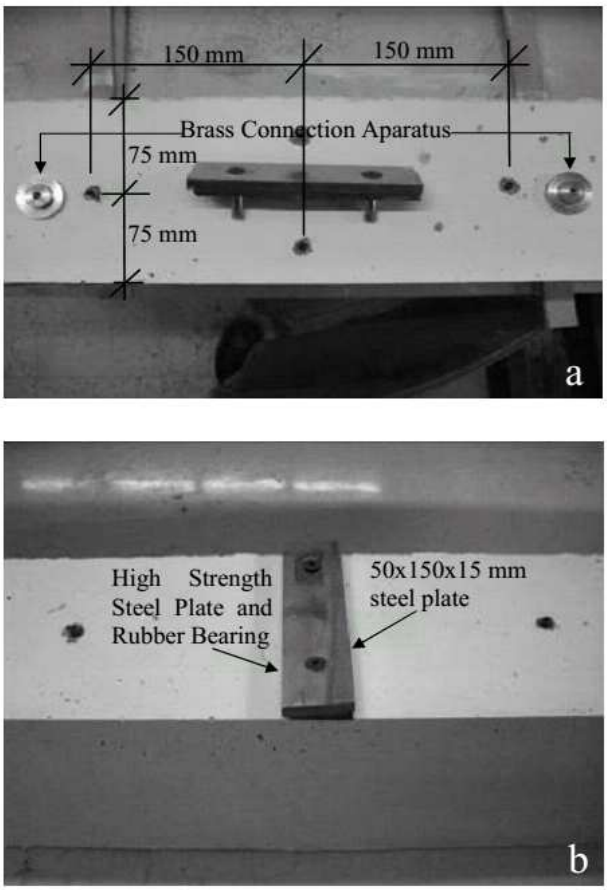

Fig. 4 Measuring Devices Preparation of Specimens for Impact Test

a) ICP Model 353B02 accelerometer

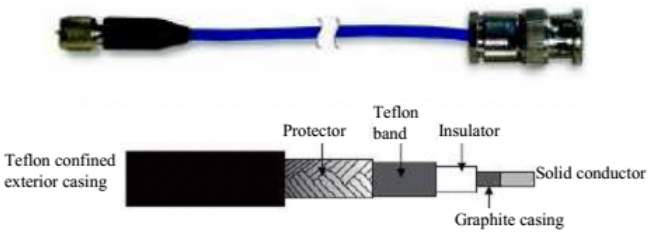

b) 003A20 model cable

c) NI 9233-USB-9162 data logger

Fig. 5 Measurement Devices of Impact Test

2.2. Experimental results

The experimental study has been conducted by carrying out static loading and dynamic impact loading tests on six concrete beam specimens. The failure patterns obtained from these tests are shown in Fig. 6 and the load - displacement graphs are presented in Fig. 7. The maximum and minimum accelerations, velocity and displacement measurements are presented in Table 2, and the load carrying capacity, stiffness and energy dissipation capacity are given in Table 3. Load carrying capacities of the specimens' were the values at which failure of the specimen was started. As can be seen from the load - displacement graphs that were given in Figure 7, stiffness values can be calculated as the ratio of maximum load carrying capacity to displacement value at that point. Stiffness values can also be defined as the slope of the line that connects maximum load carrying capacity point to origin of the load-displacement graph. Energy dissipation capacities are calculated by using the areas under the load-displacement curves. These values are showed that how much energy can be dissipated by the specimens.

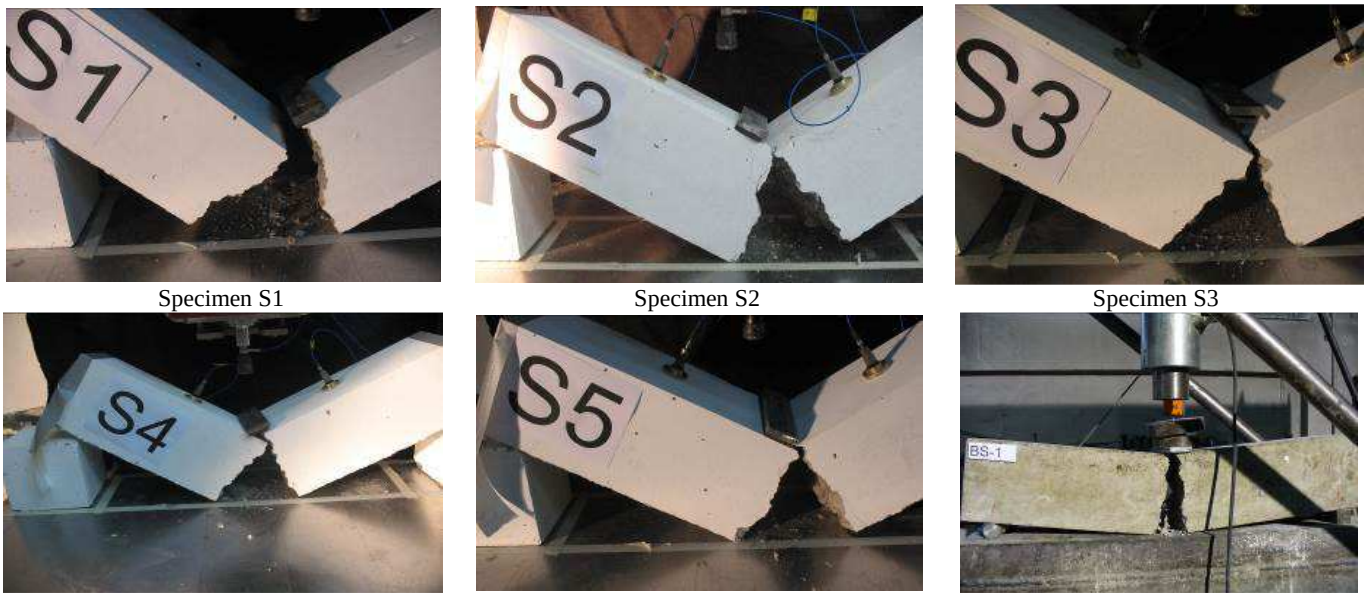

Specimen S1 Specimen S2 Specimen S3

Specimen S4 Specimen S5 Specimen BS1

Fig. 6 Test Specimens after Failure

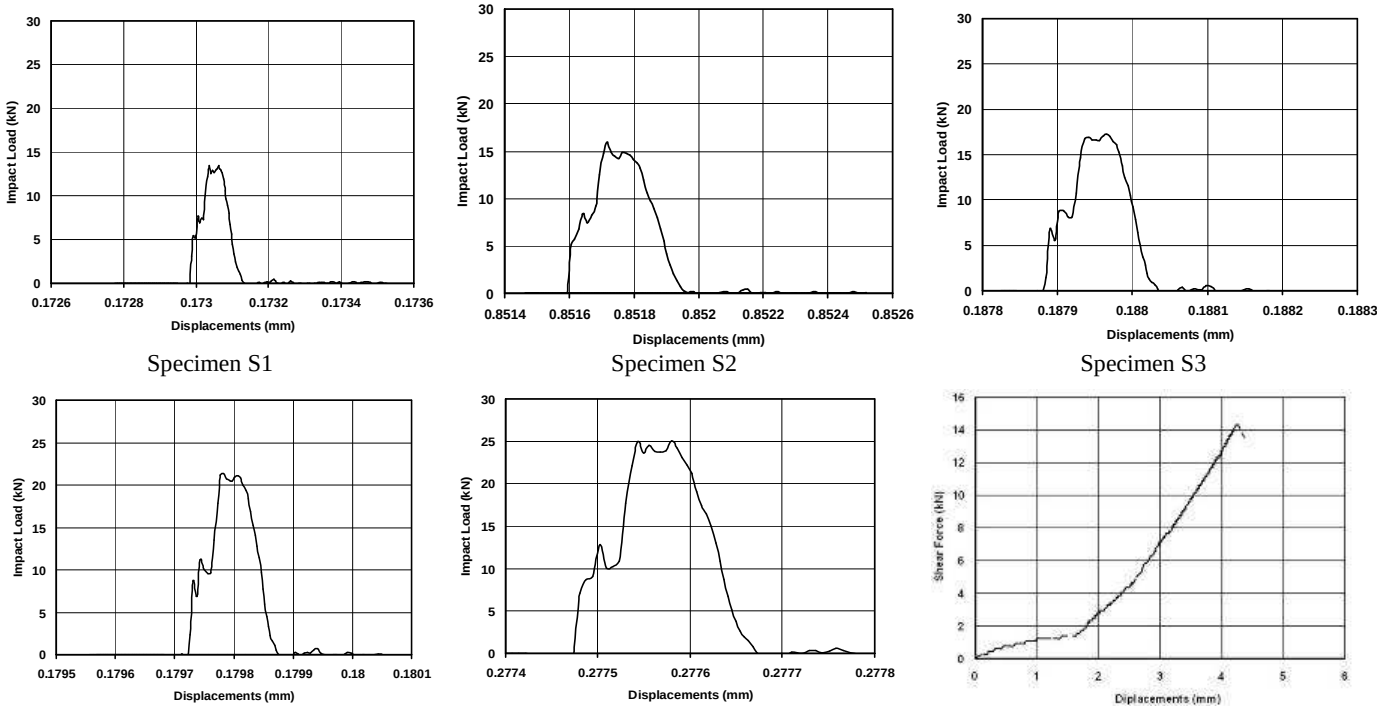

Specimen S1 Specimen S2 Specimen S3

Specimen S4 Specimen S5 Specimen BS1

Fig. 7 Load Displacement Graphs for Specimens

Table 2 Impact Test Results

Spec. No	Maximum Acceleration (g)				Failure Acceleration (g)				Acceleration Reduction (%)				Velocity at Failure(m/sn)		Displacement at Failure (mm).	
	Left		Right		Left		Right		Left		Right					
	Max.	Min.	Max.	Min.	Max.	Min.	Max.	Min.	Max.	Min.	Max.	Min.	Min.	Max.	Min.	Max.
1	260.47	-272.92	143.41	-213.94	166.00	-195.28	83.15	-177.80	57	40	72	20	-0.320	0.345	-0.290	1.446
2	132.41	-137.54	176.95	-175.83	53.90	-116.80	89.10	-165.29	146	18	99	6	-0.429	0.370	-0.384	1.831
3	157.39	-154.51	123.76	-142.25	76.50	-123.92	69.06	-120.81	106	25	79	18	-0.526	0.392	-0.517	1.932
4	190.10	-212.89	158.55	-264.10	145.68	-118.13	154.88	-250.30	30	80	2	6	-0.548	0.426	-0.553	2.265
5	158.09	-258.67	199.70	-238.81	158.10	-235.68	184.77	-213.78	20	10	8	12	-0.574	0.585	-0.589	2.507

BS1 test specimen (Spec. no: 6) was failed at a static load level of 14.35 kN with a stiffness of 3.38 kN/mm, maximum displacement of 4.35 mm and energy dissipation capacity of 22.15 kN-mm. Although the stiffness of this test specimen is quite low compared to other specimens, the failure load takes place between the failure load levels of S2 and S1 specimens. The stiffness of specimens S1 to S5 are about 65000 times greater than the stiffness of BS1 specimen. The reason of this notable increase in stiffness of beams is the short duration of impact loading. The increase in the height of hammer increased the impact load on the specimens and the maximum load capacity. The maximum load capacity of BS1 specimen is 6 percent greater than the capacity of S1 and the maximum load capacities of specimens from S2 to S5 are 11, 20, 49 and 74 percent greater than the capacity of BS2, respectively.

The energy dissipation capacity of BS1 specimen is between the capacities of S4 and S5 specimens. It is 13 percent greater than the capacity of S4 and 30 percent less than the capacity of S5 specimen. The influence of hammer height on the energy dissipation capacity is obvious and the smaller hammer height resulted in a less energy dissipation capacity. The energy dissipation capacities of S1, S2 and S3 are 48, 35 and 26 percent less than the capacity of BS1 specimen, respectively.

An increase in the hammer height resulted in an increase in the velocity and displacement measurements obtained from the accelerometers as shown in Table 2. The largest velocity and displacement value was obtained for S5 specimen, and the smallest velocity and displacement value was obtained for S1.

Table 3 Experimental Results

Spec No.	Maximum Load (kN)	Stiffness (kN/mm)	Energy Dissipation Capacity (kN-mm)
1	13.45	15954.5	11.45
2	15.94	132863.6	14.36
3	17.27	287891.2	16.31
4	21.31	302063.2	19.16
5	25.02	357403.9	28.80
6	14.35	3.38	22.15

3. Numerical Study

The numerical analysis was carried out using ANSYS Explicit Structural for both the static loading and the dynamic impact loading on plain concrete beam. This widely used software is capable of solving problems including impact and material failure using a Lagrange solver. Users can run the software as part of ANSYS workbench environment including automatic contact surface definition and with detailed material models which can be selected from the explicit material library.

3.1. Static case

The Hex-dominant method was used to obtain the entire mesh. The method can also use tetrahedral and pyramid shaped elements if necessary. The finite element model of concrete beam specimen consists of 792 hexahedral finite elements and 1127 nodes as shown in Fig. 8-a without any tetrahedral and pyramid shaped elements for the static case.

The boundary condition of lower right end of the beam was implemented as zero displacements in horizontal and vertical directions, and the lower left end was constrained to move only in *x* direction. The actual load was simulated using a pressure load which was distributed over an area of 50 mm x 150 mm located at the mid-span and the top face of the geometry as shown in Fig. 8-b.

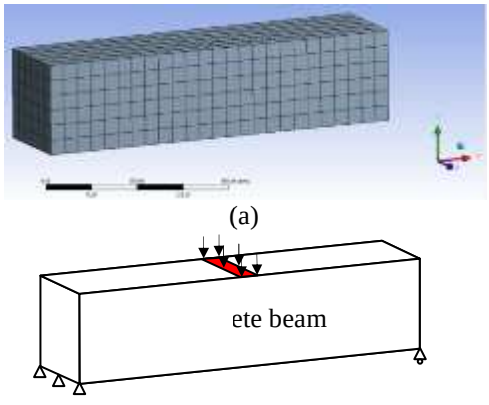

Fig. 8 a) Finite element mesh, b) Boundary conditions and loading for the static loading case

The concrete was modeled using explicit type CONCRETE-L material. The parameters including the Drucker-Prager Strength data which is applicable to

frictional materials such as soil, rock, and concrete are summarized in Table 4. The Drucker-Prager model uses the outer cone approximation to the Mohr-Coulomb law [24, 25]. The yield function *f* in the Drucker-Prager model is defined as Equation 1. The Drucker–Prager yield criterion is a pressure-dependent model for determining whether a material has failed or undergone plastic yielding. The criterion was introduced to deal with the plastic deformation of soils. It and its many variants have been applied to rock, concrete, polymers, foams, and other pressure-dependent materials. The Drucker–Prager yield criterion has the form where is the first invariant of the Cauchy stress *(I_1)* and is the second invariant of the deviatoric part *(J_2)* of the Cauchy stress.

$$f = \alpha I_1 + \sqrt{J_2} - k \tag{1}$$

where α and k are the material yield parameters determined using internal friction, ϕ and cohesion c, of the material as Equation 2.

$$\alpha = \frac{2\sin\phi}{\sqrt{3}(3-\sin\phi)}, k = \frac{6c\cdot\cos\phi}{\sqrt{3}(3-\sin\phi)} \tag{2}$$

ANSYS explicit materials library allows users to model brittle materials using certain yield stress functions such as Drucker-Prager strength linear, Drucker-Prager strength stassi, and Drucker-Prager strength piecewise. In case of CONCRETE-L, Drucker-Prager strength piecewise is utilized for which the yield stress is a linear function of pressure. The yield stress and pressure values of Drucker-Prager Strength piecewise used in the calculations were summarized in Table 4.

Table 4 Concrete-L material properties

Property	Value	Unit
Density	2440	kg m^{-3}
Shear Modulus	11200	MPa
Maximum Tensile Pressure	-1,8	MPa
Drucker-Prager Strength Data	Pressure (Pa)	Yield Stress (Pa)
	0	2.46E+7
	8E+7	1.1E+8
	1.1E+8	1.6E+8
	2E+8	1.9E+8

Comparison of experimental and numerical load-displacement graphs is given in Fig 9. The applied load was increased from zero to the ultimate load capacity in a time interval of 1.1 seconds. Three different load-time profiles were considered as shown in Fig. 9-b. First one was chosen similar to the shear force – time variation in the experimental study. The second one is a linearly increasing loading with time. The third loading was chosen similar to the shear force-displacement graph obtained from the experiment. The duration of applied loading is about 500 times longer than the impact loading, but it is shorter than of the loading in the experiments.

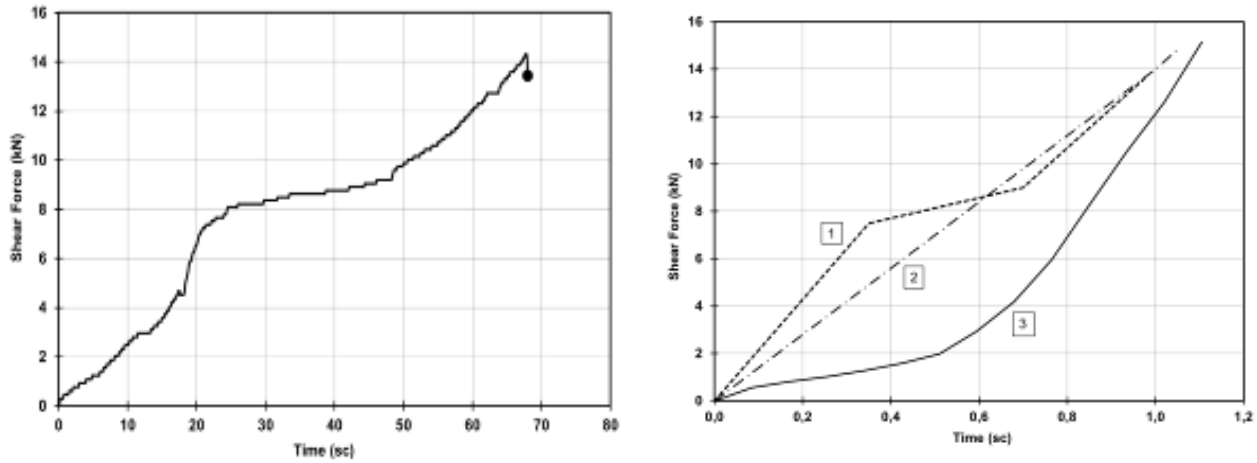

(a) (b)

Fig. 9 Variation of applied shear force with time for a) Experimental study, b) Numerical analysis

3.2. Drop weight impact case

Using the hex-dominant meshing method, the geometry of entire model was discredited into 3615 (97.9%) eight-point hexahedral elements, 69 (1.9%) five-point pyramid elements, and 10 (0.2%) tetrahedral elements as shown in Fig. 10-a. The dominant element edge size for concrete beam is 25 mm. Support blocks were discredited into hexahedrons whose minimum edge length is 10 mm and maximum edge length is 30 mm. Drop weight was also divided into hexahedral elements. Steel plate and the rubber under this plate have common nodes. The entire finite element model has 5103 nodes.

Contact elements were used for the contacting surfaces between beam and support blocks as shown in Fig. 10-b. The type of contact is frictionless. Another contact element set was located between rubber and concrete beam. The behavior of this contact is set to fully-bonded.

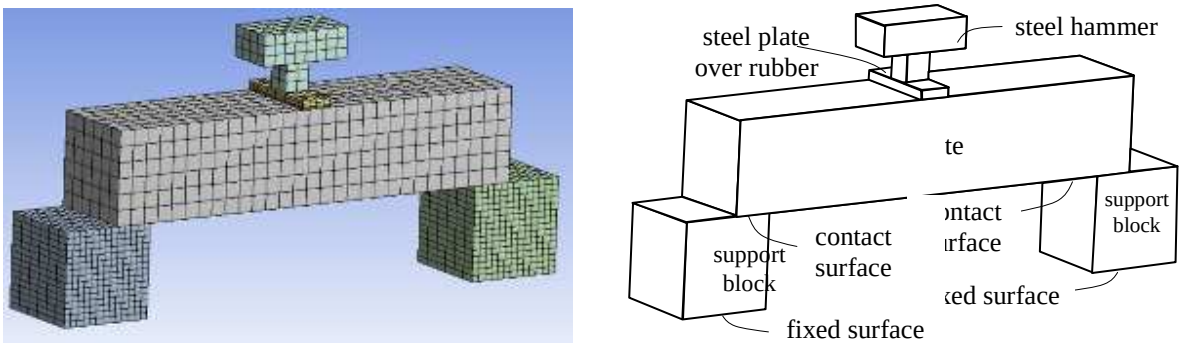

(a) (b)

Fig. 10 a) Finite element mesh, b) boundary conditions and loading for the dynamic impact loading case

ANSYS explicit materials library has two concrete materials named as CONC-35 and CONC-140 in addition to CONCRETE-L material model. These models have advanced plasticity options for brittle materials covered by the RHT concrete strength [26] which is expressed in terms of pressure dependent initial elastic yield surface, failure surface and residual friction surface in the stress space. The mathematical description of RHT model, descriptions of the parameters such as polynomial equation of state (EOS) parameters, damage parameters, and failure surface parameters and their default values corresponding to standard 35 MPa concrete can be found in [27].

The data for the analysis of concrete with cube strengths of 35 MPa and 140 MPa are ready to use in the library. The concrete materials with different cube strength values can be derived by changing the cube strength and the remaining values will scale proportionately [25]. In the present work, the cube strength of CONC-35 was set to 24.6 MPa for the concrete material for which the density value was set to 2350 kg/m^3. The shear modulus of concrete was calculated as 11200 MPa which is 40 percent of the concrete's modulus of elasticity which is 28000 MPa. Initial compaction pressure was considered as 1.67E+7 Pa. Compressive strain rate exponent α, and tensile strain rate exponent δ, were calculated as 0.042 and 0.044, respectively using the following Equation 3 [28],

$$\alpha = \frac{1}{(5+\frac{3}{4}f_C)}, \delta = \frac{1}{(10+\frac{1}{2}f_C)} \quad (3)$$

where f_c is the uniaxial compressive strength of the concrete. Other parameters were used with their default values. The RHT concrete model parameters used in the present numerical analysis are summarized in Table 5.

Table 5 Parameters for the RHT concrete model

RHT concrete Strength	
Shear modulus	1.12E+10 (Pa)
Compressive strength (fc)	2.46E+07 (Pa)
Tensile strength (ft/fc)	0.1
Shear strength (fs/fc)	0.18
Intact failure surface constant A	1.6
Intact failure surface exponent n	0.61
Tens./Comp. meridian ratio Q2.0	0.6805
Brittle to ductile transition BQ	0.0105
Hardening Slope	2
Elastic strength/ft	0.7
Elastic strength/fc	0.53
Fractured strength constant B	1.6
Fractured strength exponent M	0.61
Compressive strain-rate exponent α	0.042
Tensile strain-rate exponent δ	0.044
Max. fracture strength ratio	1E+20
Use CAP on elastic surface?	Yes
RHT Concrete Failure	
Damage constant D1	0.04
Damage constant D2	1
Minimum strain to failure	0.01
Residual shear modulus fraction	0.13
Polynomial EOS	
Bulk modulus A1	3.527E+10 (Pa)
Parameter A2	3.958E+10 (Pa)
Parameter A3	9.04E+09 (Pa)
Parameter B0	1.22
Parameter B1	1.22
Parameter T1	3.527E+10 (Pa)
Parameter T2	0
P-alpha EOS	
Solid density	2750 (kg/m^3)
Porous sound speed	2920 (m/s)
Initial compaction pressure	1.67E+07 (Pa)
Solid compaction pressure	6E+09 (Pa)
Compaction exponent, n	3
Density	2350 (kg/m^3)
Specific heat	654 (J/kgC)

The steel hammer was modeled using the Structural Steel material whose properties are given in Table 6. Rubber between steel plate and concrete beam were modeled using a material whose details are also given in Table 6.

Table 6 The material properties of structural steel and rubber

	Structural Steel		Rubber	
Property	Value	Unit	Value	Unit
Density	7580	kg m^{-3}	1230	kg m^{-3}
Young's Modulus	2E+11	Pa	2.2E+7	Pa
Poisson's Ratio	0.3		0.45	
Bulk Modulus	1.667E+11	Pa	7.333E+7	Pa
Shear Modulus	7.692E+10	Pa	7.586E+6	Pa

Motion of the hammer from its rest position up to the instant just before the impact was considered as constantly accelerated motion. The observed duration of this motion is given in Table 1. Because of the long run time of the numerical solution, the FE analysis was started from the instant that the hammer is located at 1 mm distance above from the top of concrete beam with an initial vertical speed. The speeds of steel hammer calculated from the uniformly accelerated rectilinear motion formula at the instant just before the impact are 2553, 2672, 2797, 3030, 3185 mm/s for specimens S1 to S5, respectively.

4. Comparison of Numerical Results and Experimental Results

Response of plain concrete beam to the given static loading is represented by the graph of applied force versus midpoint displacement as shown in Fig. 11. Here, the displacements obtained from FE analysis using the load-time profiles indicated by 1, 2, and 3 are plotted. Displacement response of the concrete beam obtained from the FE analysis are similar to the curves of load-time graphs shown in Fig. 9-b, i.e. a linearly increasing load-time relation resulted in a nearly linear force-displacement graph.

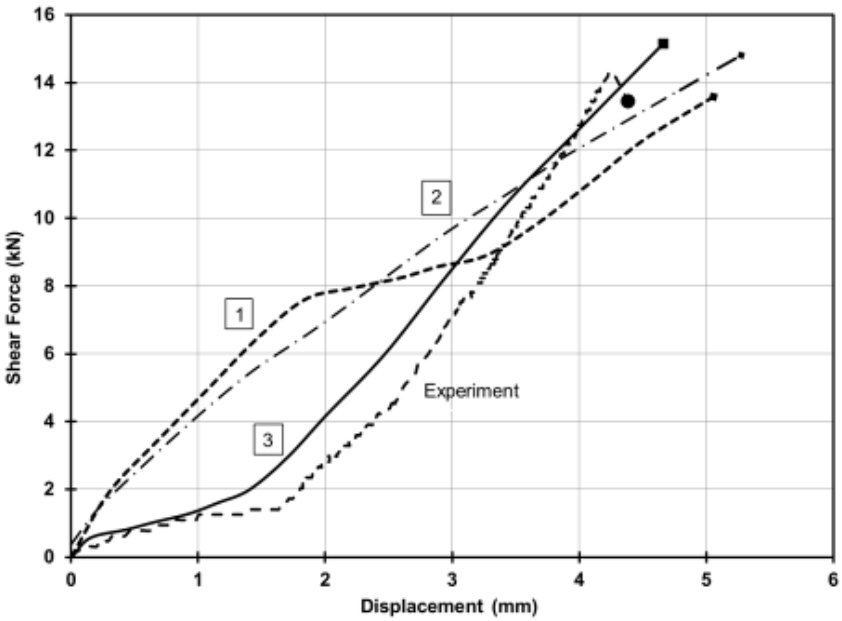

Fig. 11 Shear force – displacement curves obtained from experimental study and FE analysis for static loading test

The maximum and minimum values of displacement, velocity and acceleration calculated at the points representing the locations of accelerometers on the finite element mesh and those obtained from the experimental study are given in Table 7. The percent difference between the experimental results and the FE model results changes between 0.5% and 62%.

Table 7 Comparison of FE model and experimental values of displacement, velocity and acceleration

		FE model	Experiment	Difference (%)
S1	Displacement (mm)	−0.258	−0.290	12.4
		+2.236	+1.446	54.6
	Velocity (mm/s)	−366	−320	14.4
		+360	+345	4.3
	Acceleration (m/s^2)	+134.15 g	+143.41 g	6.5
		−217.64 g	−213.94 g	1.7
S2	Displacement (mm)	−0.589	−0.384	53.4

	Velocity (mm/s)	+2.588	+1.831	41.3
		−693	−429	61.5
	Acceleration (m/s^2)	+383	+370	3.5
		+132.93 g	+176.95 g	24.9
	Displacement (mm)	−225.59 g	−175.83 g	28.3
		−0.653	−0.517	26,3
S3	Velocity (mm/s)	+2.591	+1.932	34.1
		−737	−526	40.1
	Acceleration (m/s^2)	+380	+392	3.1
		+142.41 g	+157.39 g	9.5
	Displacement (mm)	−237.61 g	−154.51 g	53.8
		−0.648	−0.553	17.2
S4	Velocity (mm/s)	+2.836	+2.265	25.2
		−753	−548	37.4
	Acceleration (m/s^2)	+403	+426	5.4
		+143.01 g	+158.55 g	9.8
	Displacement (mm)	−242.61 g	−264.10 g	8.1
		−0.669	−0.589	13.6
S5	Velocity (mm/s)	+3.003	+2.507	19.8
		−778	−574	35.5
	Acceleration (m/s^2)	+384	+585	34.4
		+158.92 g	+158.09 g	0.5
		−262.90 g	−258.67 g	1.6

The examples of variation of displacement, velocity and acceleration with time obtained from FE analysis of specimen S1 and S5 are plotted as shown in Fig. 12. Comparison of analytical FE results and experimental results acceleration, displacement and velocity for specimen S3 are given in Fig. 13. The normal stresses along the x-axis are plotted in Fig. 14 of the specimen S5 and shear stresses are plotted in Fig. 15 for an example. Shear stress distribution obtained from FE analysis is consistent with the failure plane of specimen in the experiments and maximum shear stress is concentrated in a region close to the application point of loading.

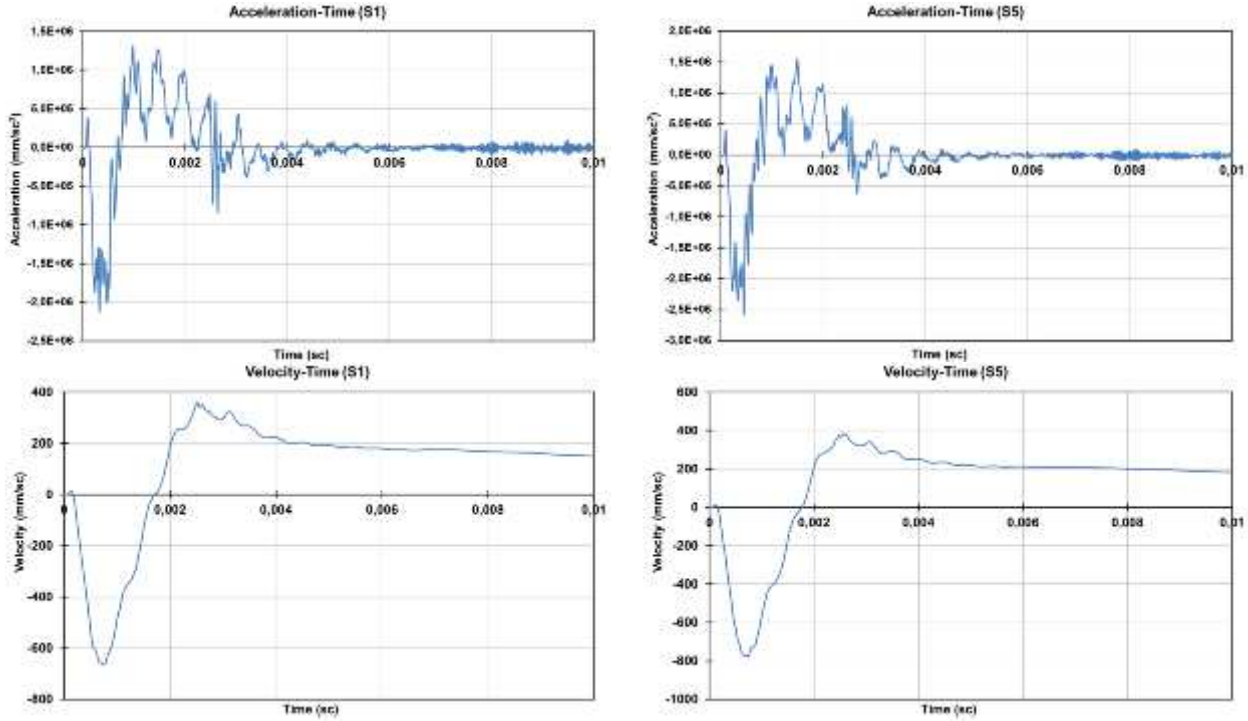

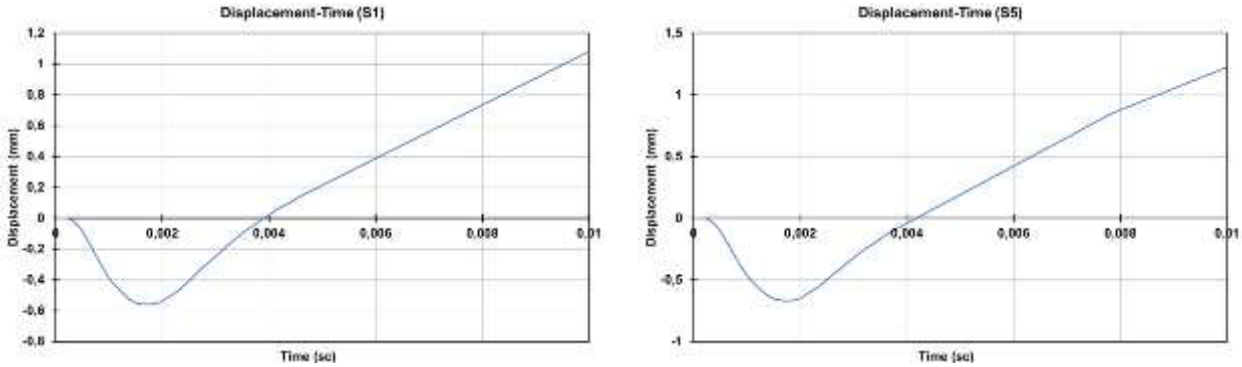

Fig. 12 Displacement, velocity, and acceleration graphs for Specimen S1 and S5 obtained from FE model

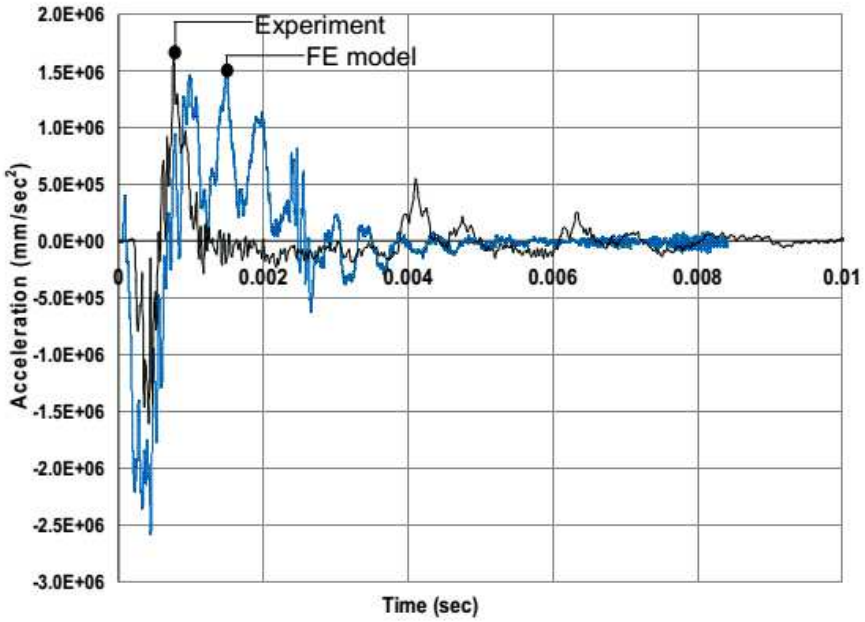

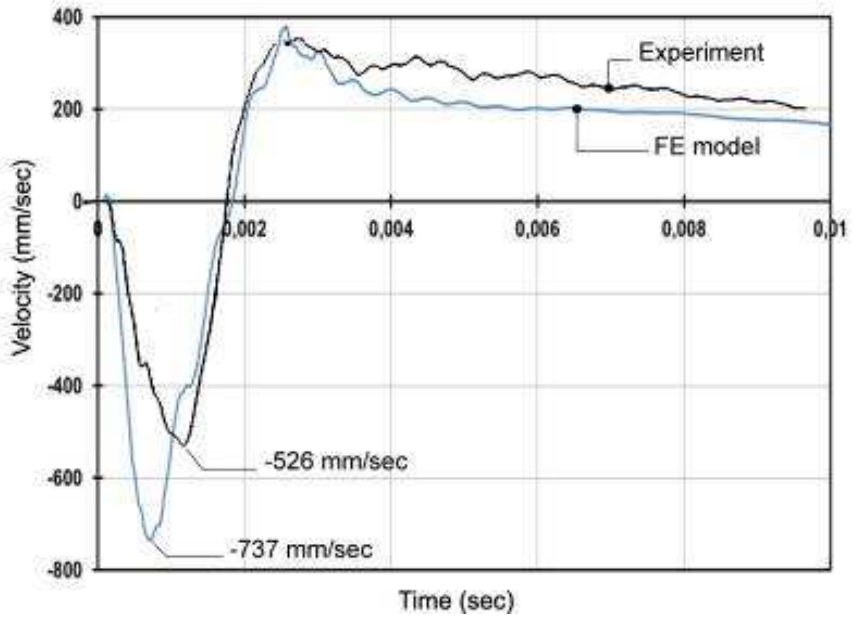

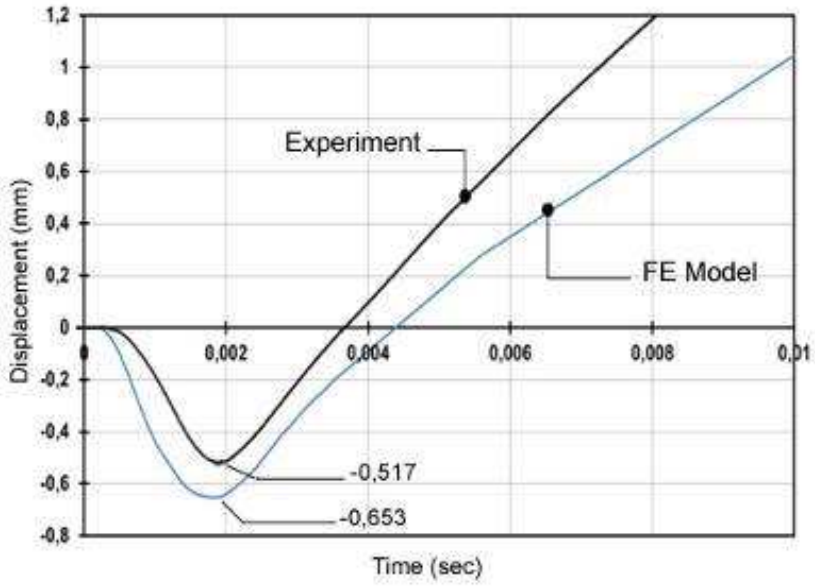

Fig. 13 Comparison of acceleration, displacement and velocity variations of S3 with time

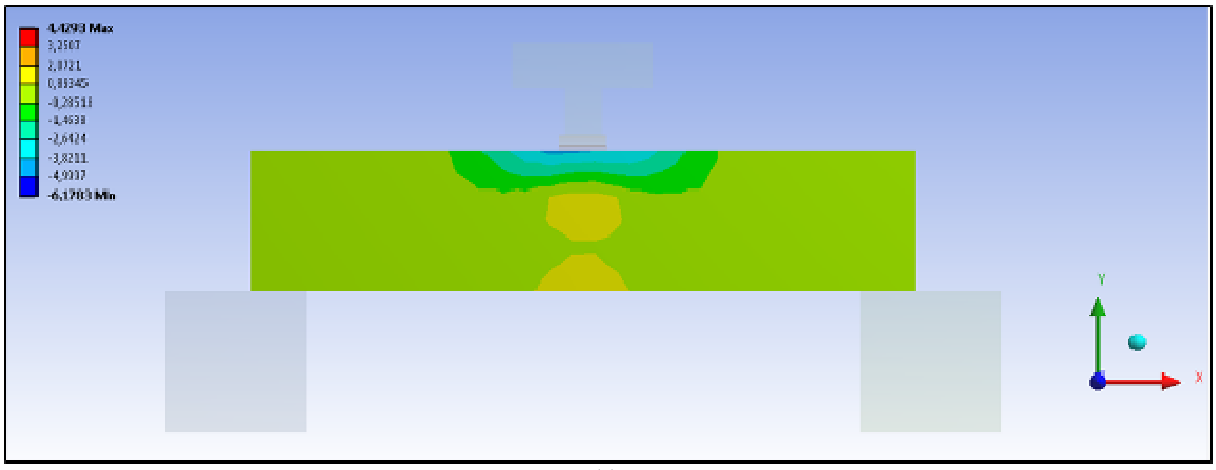

(a)

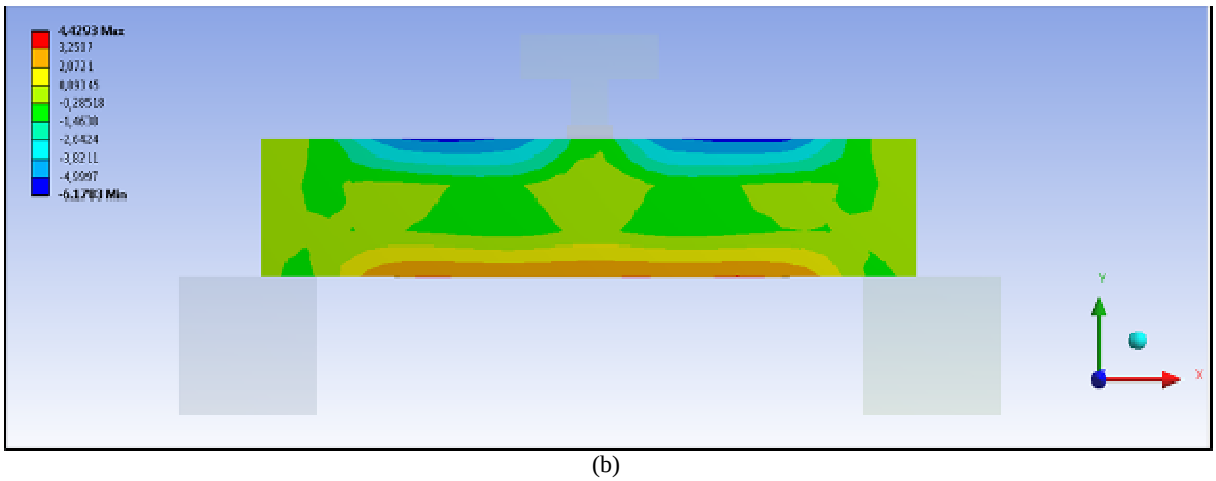

(b)

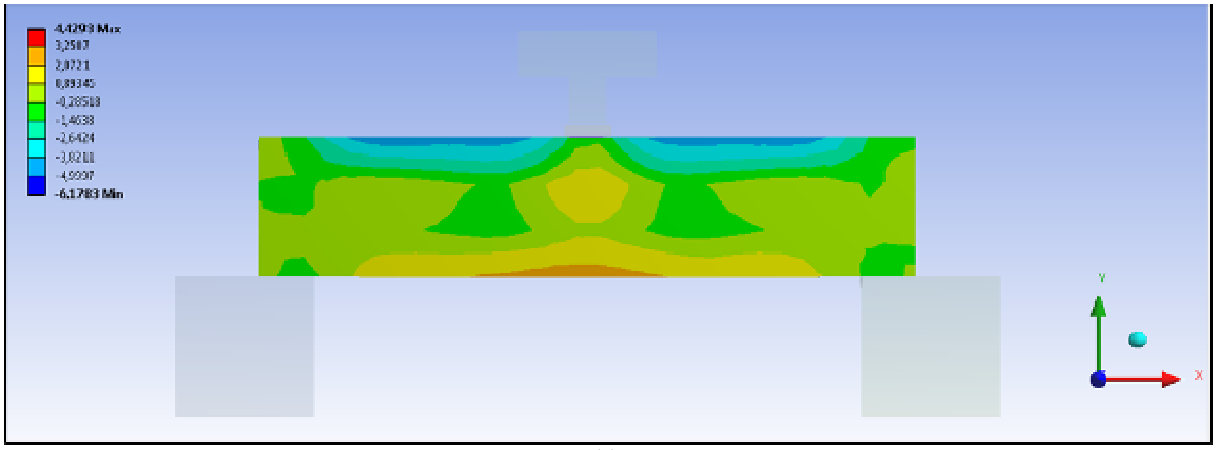

(c)

Figure 14. S5 specimen normal stress along *x* for a) at 0.000344 sec b) at 0.00103 c) at 0.00172 sec

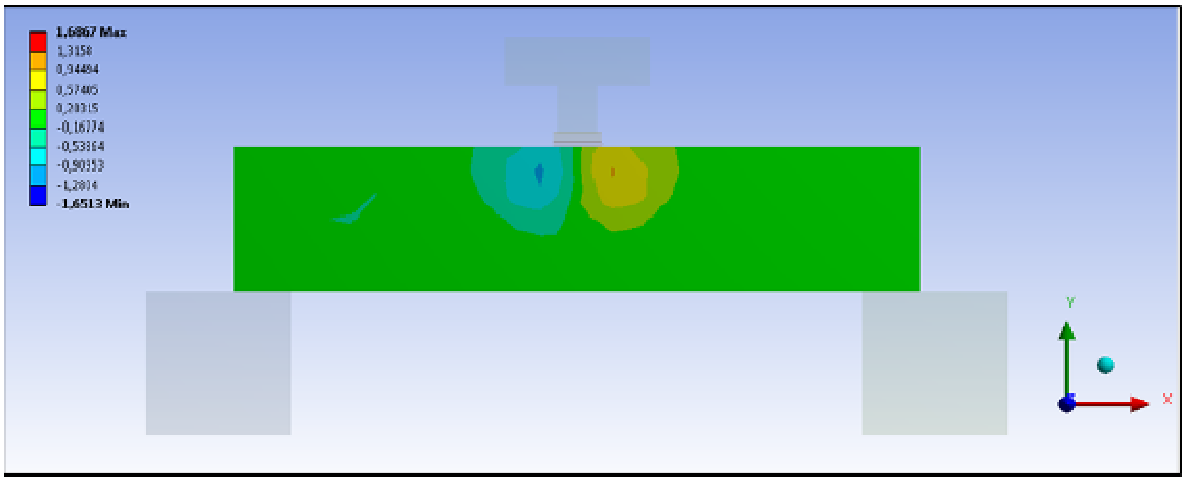

(a)

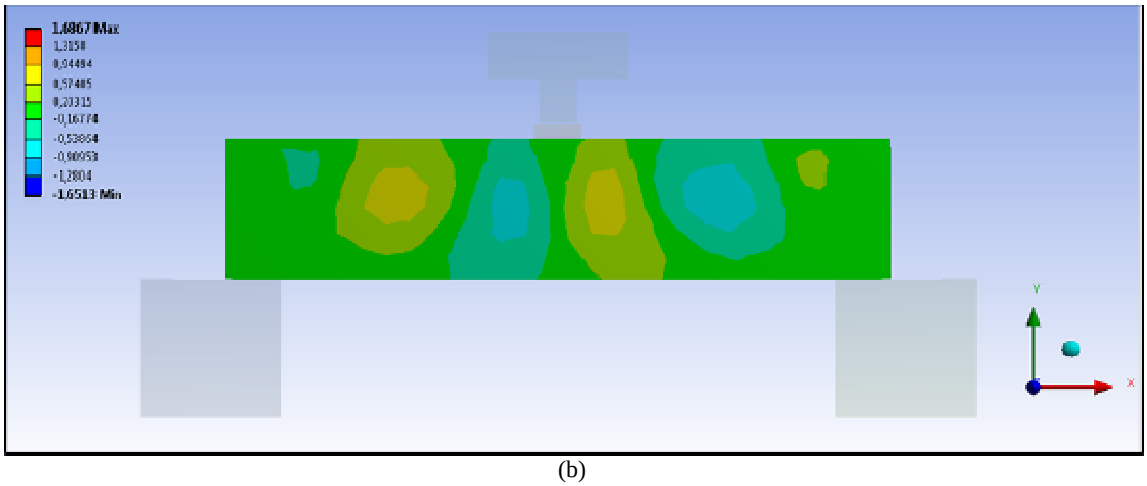

(b)

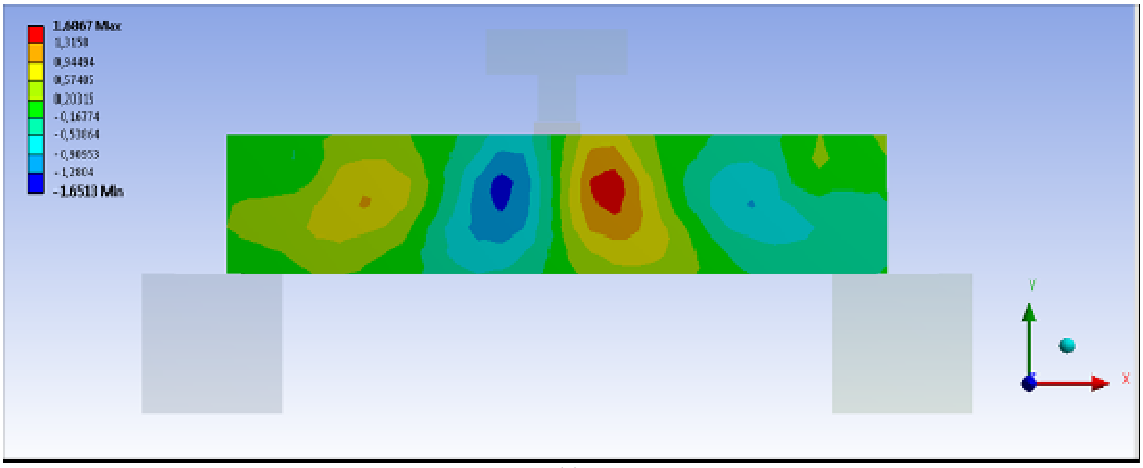

(c)

Figure 15. S5 specimen shear stress plots for a) at 0.000344 sec b) at 0.00103 c) at 0.00172 sec

5. Conclusion and Discussion

Concrete beam specimens with same geometry, concrete mixture and compression strength were tested by applying low velocity impact load and three-point static load. Main variables of the experiments were the type of loading and the hammer height for impact loading. Total six concrete beam specimens, one for static loading case and five for dynamic loading case with five different drop weight heights, were tested. Finite element analyses of the concrete beams modeled in ANSYS were carried out and the results were compared obtained from the experiments. The conclusion is presented as follows,

- The change of loading type is quite affective on energy dissipation capacity, stiffness, maximum load and failure mode of concrete beams.
- The initial stiffness of concrete beams has increased significantly in the case of impact load, for which the duration of applied load is very short. Initial stiffness of the specimens under impact loading is about 65000 times greater with respect to static loading case. Initial stiffness of the concrete beams is increased with an increase in the drop weight height.
- Type of loading influences load carrying capacity of the concrete beams. Load carrying capacity of the test specimens has increased with increasing drop weight height. The S1 test specimen having the minimum drop weight height and the BS1 test specimen exhibited a close load carrying capacity. The S5 test specimen with a drop height of 500 mm has 74 percent greater load carrying capacity with respect to the BS1 test specimen.
- The energy dissipation capacity has increased with the increase in drop weight height. The specimen tested under static loading has larger midpoint displacement with respect to the impact loading case when it was reached to its load carrying capacity which falls behind the values for other specimens. Because of short duration of impact loading, smaller midpoint displacements and greater load carrying capacity values were observed. Only the test specimen S5 has 30 percent greater energy dissipation capacity than the specimen tested under static loading. The concrete beams have a potential increasing energy dissipation capacity with increasing impact velocity for the low velocity impact loading.
- During the impact tests, velocity and displacement values of points on the test specimens increased with increasing drop weight height.
- Finite element analysis of concrete beams under static and dynamic loading has been carried out using ANSYS Explicit STR. Drucker-Prager Strength piecewise material model for the static loading case and advanced plasticity options for brittle materials covered by the RHT concrete strength for the impact loading case were used in the analyses.
- Three different loading rates of static loading were tested for the finite element analysis of concrete beam model. These three cases, at the failure load level, yield close midpoint displacement values, but a shear force-displacement curve similar to the experimental result can only be obtained for the third loading rate case.
- A comparison between experimental and FE displacement results of the concrete beams subjected to dynamic impact loading shows that there exist 35% and 24% average difference for maximum and minimum displacement values, respectively. The average difference between experiment and FE analysis for maximum and minimum velocity values are 10% and 38%, respectively. The average difference for maximum and minimum acceleration values are 19% and 10%, respectively. FE model which can be used in the design procedure is obtained with consistent results.
- In addition to the proper maximum and minimum values of acceleration, velocity and displacement, similar curves representing the variation of these parameters with time have been obtained from the FE analysis.
- Shear stress distribution obtained from FE analysis is consistent with the failure plane of specimen in the experiments and maximum shear stress is concentrated in a region close to the application point of loading.

References

[1] Goldsmith W. Impact: The Theory and Physical Behavior of Colliding Solids, London Edward Arnold Limited, 1960, pp. 145-240.

[2] Murtiadi S. Behavior of high-strength concrete plates under impact loading, Master Thesis, Faculty of Engineering and Applied Science, Mernorial University of Newfoundland, 1999.

[3] Kishi N, Mikami H, Matsuoka KG, Ando T. Impact behavior of shear-Failure-type RC beams without shear rebar, International Journal of Impact Engineering, 2002, Vol. 27, pp. 955-968.

[4] Bhatti AQ, Kishi N, Mikami H, Ando T. Elasto-plastic impact response analysis of shear-failure-type RC beams with shear rebars, Materials and Design, 2009, Vol. 30, pp. 502-510.

[5] Cotsovos DM, Stathopoulos N, Zeris C. Behavior of RC beams subjected to high rates of concentrated loading, Journal of Structural Engineering, 2008, Vol. 134, pp. 1839-1851.

[6] Cotsovos DM. A simplified approach for assessing the load-carrying capacity of reinforced concrete beams under concentrated load applied at high rates, International Journal of Impact Engineering, 2010, Vol. 37, pp. 907-917.

[7] Zineddin M, Krauthammer T. Dynamic response and behavior of reinforced concrete slabs under impact loading, International Journal of Impact Engineering, 2007, Vol. 34, pp. 1517-1534.

[8] Hummeltenberg A, Beckmann B, Weber T, Curbach M. Investigation of concrete slabs under impact load, Applied Mechanics and Materials, 2011, Vol. 82, pp. 398-403.

[9] Kishi N, Komuro M, Takeda M. Numerical simulation of the dynamic response behavior of an RC portal frame under road vehicle impact, Proceedings of the 9th International Conference on Shock and Impact Loads on Structures, 2011, pp. 443-448.

[10] Serrano-Perez JC, Vaidya UK, Uddin N. Low velocity impact response of autoclaved aerated concrete/CFRP sandwich plates, Composite Structures, 2007, Vol. 80, pp. 621-630.

[11] Liew JYR, Sohel KMA, Koh CG. Impact tests on steel-concrete-steel sandwich beams with lightweight concrete core, Engineering Structures, 2009, Vol. 31, pp. 2045-2059.

[12] Kantar E, Anil O. Low velocity impact behavior of concrete beam strengthened with CFRP strip, Steel and Composite Structures, 2012, Vol. 12, pp. 207-230.

[13] Kaewunruen S, Remennikov AM. Impact capacity of railway prestressed concrete sleepers, Engineering Failure Analysis, 2009, Vol. 16, pp. 1520-1532.

[14] Zhang XX, Ruiz G, Yu RC. A new drop-weight impact machine for studying fracture processes in structural concrete, Strain, 2010, Vol. 46, pp. 252-257.

[15] Bischoff PH, Perry PH. Impact Behavior of Plain Concrete Loaded in Uniaxial Compression, Journal of Engineering Mechanics, 2007, Vol. 121, pp. 685-693.

[16] Grote DL, Park SW, Zhou M. Dynamic behavior of concrete at high strain rates and pressures: I. experimental characterization, International Journal of Impact Engineering, 2001, Vol. 25, pp. 869-886.

[17] Park SW, Xia Q, Zhou M. Dynamic behavior of concrete at high strain rates and pressures: II. numerical simulation, International Journal of Impact Engineering, 2001, Vol. 25, pp. 887-910.

[18] Kantar E, Erdem RT, Anil O. Nonlinear finite element analysis of impact behavior of concrete beam, Mathematical and Computational Applications, 2011, Vol. 16, pp. 183-193.

[19] Travaš V, Ožbolt J, Kožar I. Failure of plain concrete beam at impact load: 3D finite element analysis, International Journal of Fracture, 2009, Vol. 160, pp. 31-41.

[20] Bazant ZP, Prat PC. Microplane model for brittle-plastic material: I. theory, Journal of Engineering Mechanics, 1988, Vol. 114, pp. 1672-1688.

[21] Bazant ZP, Prat PC. Microplane model for brittle-plastic material: II. verification, Journal of Engineering Mechanics, 1988, Vol. 114, pp. 1689-1702.

[22] Bazant ZP, Adley MD, Carol I, Jirásek M, Akers SA, Rohani B, Cargile JD, Caner FC. Large-strain generalization of microplane model for concrete and application, Journal of Engineering Mechanics, 2000, Vol. 126, pp. 971-980.

[23] Ožbolt J, Li Y, Kožar I. Microplane model for concentre with relaxed kinematic constraint, International Journal of Solids and Structures, 2001, Vol. 38, pp. 2683-2711.

[24] Drucker DC, Prager W. Soil mechanics and plastic analysis on limit design, Quarterly Journal of Applied Mathematics, 1952, Vol. 10, pp. 157-165.

[25] ANSYS Users Manual, 2005.

[26] Riedel W, Thoma K, Hiermaier S, Schmolinske E. Penetration of reinforced concrete by beta-b-500, numerical analysis using a new macroscopic concrete model for hydrocodes, Proceedings CD-ROM of 9th International Symposium on Interaction of the Effects of Munitions with Structures, Berlin Strausberg, 1999, pp. 315-322.

[27] Borrvall T, Riedel W. The RHT concrete model in LS-dyna, 8th European LS-DYNA Users Conference, Strasbourg, France, 2011.

[28] Riedel W, Kawai N, Kondo K. Numerical assessment for impact strength measurements in concrete materials, International Journal of Impact Engineering, 2009, Vol. 36, pp. 283-293.